EMBO reports

scientific report

Structural basis of N-end rule substrate recognition in *Escherichia coli* by the ClpAP adaptor protein ClpS

Verena J. Schuenemann[1], Stephanie M. Kralik[2], Reinhard Albrecht[1], Sukhdeep K. Spall[2], Kaye N. Truscott[2], David A. Dougan[2+] & Kornelius Zeth[1++]

[1]Department of Protein Evolution, Max Planck Institute for Developmental Biology, Tübingen, Germany, and [2]Department of Biochemistry, La Trobe University, Melbourne, Australia

In *Escherichia coli*, the ClpAP protease, together with the adaptor protein ClpS, is responsible for the degradation of proteins bearing an amino-terminal destabilizing amino acid (N-degron). Here, we determined the three-dimensional structures of ClpS in complex with three peptides, each having a different destabilizing residue—Leu, Phe or Trp—at its N terminus. All peptides, regardless of the identity of their N-terminal residue, are bound in a surface pocket on ClpS in a stereo-specific manner. Several highly conserved residues in this binding pocket interact directly with the backbone of the N-degron peptide and hence are crucial for the binding of all N-degrons. By contrast, two hydrophobic residues define the volume of the binding pocket and influence the specificity of ClpS. Taken together, our data suggest that ClpS has been optimized for the binding and delivery of N-degrons containing an N-terminal Phe or Leu.

Keywords: ClpS; N-end rule pathway; N-recognin; proteolysis; ITC

EMBO reports (2009) **10**, 508–514. doi:10.1038/embor.2009.62

INTRODUCTION

Intracellular protein degradation has a crucial function in the correct maintenance of both prokaryotic and eukaryotic cells. Often, proteins destined for destruction contain amino- or carboxy-terminal recognition motifs (Baker & Sauer, 2006). One example of an N-terminal recognition motif is the N-end rule, which states that an N-terminal residue might be either stabilizing or destabilizing (N-degron), and this determines the half-life of the protein (Varshavsky, 1996; Mogk *et al*, 2007). In eukaryotes, this N-end rule pathway is known to have an important function in various cellular processes, including chromosome segregation and cardiovascular development (Tasaki & Kwon, 2007). In humans, destabilizing residues are hierarchical and can be divided into three classes: primary (type 1 (Arg, Lys or His) or type 2 (Ile, Leu, Phe, Tyr or Trp); see Fig 1D), secondary (Asp, Glu or oxidized Cys) and tertiary (Asn, Gln or Cys). In eukaryotes, a primary N-degron is recognized by specific members of the E3 ligase family—also known as N-recognins—resulting in substrate ubiquitination and subsequent degradation by the 26S proteasome. Although bacteria do not have the necessary components for ubiquitination, many of the remaining components of the N-end rule pathway are conserved. In *Escherichia coli*, the N-end rule pathway is also hierarchical; however, destabilizing residues are either primary (Leu, Phe, Tyr and Trp; see Fig 1D) or secondary (Arg and Lys). Secondary destabilizing residues are responsible for the attachment of primary destabilizing residues through the conjugation of Leu or Phe to an N-terminal Arg or Lys by the L/F-transferase (LFTR; Soffer, 1974; Tobias *et al*, 1991; Watanabe *et al*, 2007). Interestingly, in *E. coli*, the adaptor protein ClpS, which is predicted to share secondary structure with the type 2 binding site of eukaryotic N-recognins, has been proposed to bind to primary destabilizing residues and deliver them to ClpAP for degradation (Tobias *et al*, 1991; Lupas & Koretke, 2003; Erbse *et al*, 2006). Although ClpS and N-recognins are predicted to share secondary structure features within the 'ClpS' domain, their sequence similarity is limited in this region, which might account for their divergence in substrate specificity. Importantly, the recognition components of the N-end rule, regardless of their origin, must both show specificity and also demonstrate structural plasticity to bind to the full range of primary N-degrons. For example, the bacterial recognition factor ClpS can selectively bind to Leu but not to Ile or Met, while retaining the ability to accommodate the large aromatic side chains of Phe, Trp and Tyr; so far, there is no structural information to understand how this is achieved.

Here, we describe three crystal structures of ClpS in complex with various model N-end rule peptides. Collectively, the structural and thermodynamic data determined by using isothermal titration calorimetry (ITC) provide considerable insight into how an N-end rule peptide docks with its cognate recognition factor. The structural alignment of the various complexes shows that each N-end rule peptide docks to ClpS in a fixed orientation and makes several contacts with residues in the binding pocket. To determine the functional importance of these residues and to

[1]Department of Protein Evolution, Max Planck Institute for Developmental Biology, Spemannstrasse 35, Tübingen D-72076, Germany
[2]Department of Biochemistry, La Trobe University, Melbourne 3086, Australia
[+]Corresponding author. Tel: +61 3 9479 3276; Fax: +61 3 9479 2467;
E-mail: d.dougan@latrobe.edu.au
[++]Corresponding author. Tel: +49 7071 601 323; Fax: +49 7071 601 349;
E-mail: kornelius.zeth@tuebingen.mpg.de

Received 5 November 2008; revised 2 March 2009; accepted 3 March 2009; published online 17 April 2009

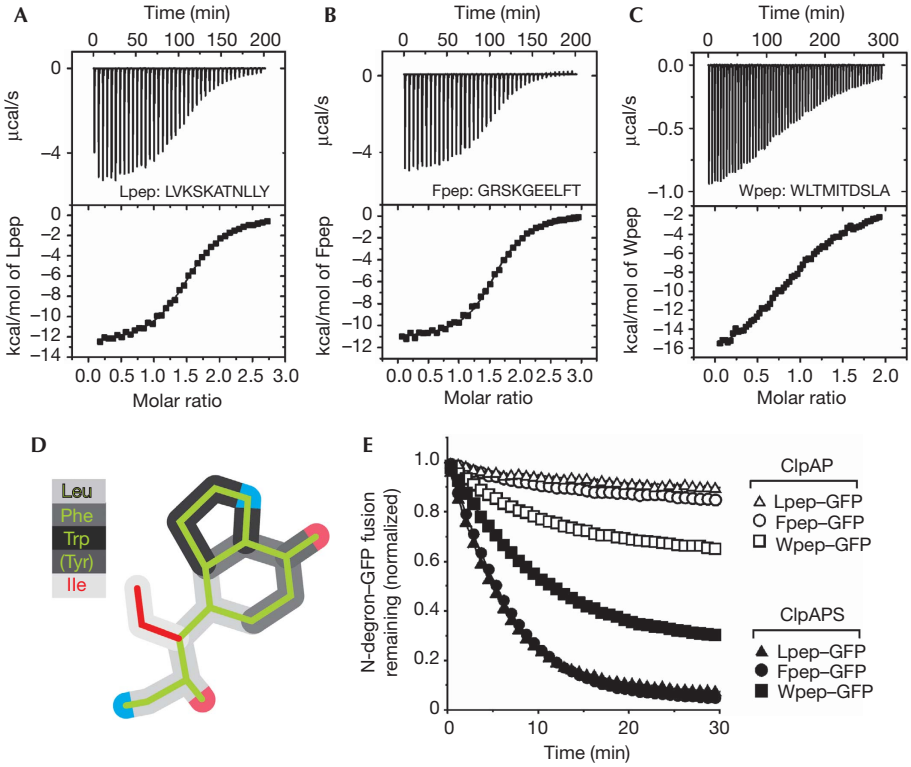

Fig 1 | Binding and degradation of model N-degrons. (**A–C**) Isothermal titration calorimetry of ClpS (0.08 mM) binding to (**A**) Lpep, (**B**) Fpep and (**C**) Wpep. (**A**) Titration of 40 injections (4 µl) of Lpep (2 mM) were performed, revealing a dissociation constant of 4.8 µM. (**B**) Titration of 50 injections (3 µl) of Fpep (2 mM) was performed, showing a dissociation constant of 3.8 µM. (**C**) Titration of Wpep (0.6 mM) was performed with 60 injections (3 µl), showing a dissociation constant of 8.1 µM. (**D**) Schematic representation of all possible type 2 destabilizing amino acids: Leu, Phe, Trp, Tyr and Ile. (**E**) The ClpAP-mediated degradation of Lpep–GFP (green fluorescent protein; triangles), Fpep–GFP (circles) and Wpep–GFP (squares) was monitored by fluorescence in the absence (open symbols) or presence (filled symbols) of ClpS.

understand better the substrate specificity of ClpS, we mutated four residues within the hydrophobic cavity of ClpS. Initially, we compared the ability of each mutant protein to deliver various model N-end rule substrates to ClpAP for degradation. Collectively, these data show that His 66 makes an essential interaction with the peptide backbone of the substrate, and removal of this interaction abolishes the ClpAP-mediated degradation of all model N-end rule substrates. By contrast, the mutation of either Met 40 or Met 62, to increase the volume of the binding pocket, enhances the rate of degradation of Wpep–GFP (green fluorescent protein) while reducing the degradation rates of Lpep–GFP and Fpep–GFP. On the basis of these data, we speculate that the ClpS substrate-binding site has been optimized for the recognition of N-degrons generated by LFTR.

RESULTS AND DISCUSSION

Biochemical analysis

To gain a detailed understanding of the interaction between ClpS and its substrate, we crystallized ClpS in complex with various N-degron peptides. The first peptide (referred to as Lpep) was derived from an N-terminal truncation of Dps (Dps6–167), a putative natural substrate of the *E. coli* N-end rule pathway (R.L. Ninnis, S.K. Spall, G.H. Talbo, K.N. Truscott and D.A. Dougan, unpublished data). The other peptides (referred to as Fpep and Wpep) were derived from model N-end rule substrates FR-linker-GFP and W-βgal, respectively (Tobias *et al*, 1991; Erbse *et al*, 2006). We used ITC to establish the binding affinity of the peptides towards the adaptor protein ClpS. Initially, we speculated that the relative affinities of the various peptides (Fig 1A–C) would be proportional to the volume of the N-terminal residue; for example, Trp (228 Å^3) > Phe (190 Å^3) > Leu (167 Å^3). Surprisingly, Wpep (K_d = 8.1 µM) showed the weakest affinity for ClpS of all the peptides and Fpep (K_d = 3.8 µM), which shows the closest correlation between the side chain (190 Å^3) and binding pocket (~200 Å^3) volume, showed the strongest affinity (supplementary Table S1 online). Interestingly, the binding stoichiometry of Lpep (Fig 1A) and Fpep (Fig 1B) to ClpS was determined to be 1.5:1, whereas Wpep (Fig 1C) showed a binding stoichiometry consistent with the structural data, in which a single peptide was bound to a unique site in ClpS. Importantly, the affinity of Fpep to ClpS was in close agreement with that determined by surface plasmon resonance (Erbse *et al*, 2006). Next, we created a set of fusion proteins, in which each N-degron peptide was attached to the N terminus of GFP (Lpep–GFP, Fpep–GFP and Wpep–GFP). As expected, the ClpAP-mediated degradation of Lpep–GFP and Fpep–GFP was ClpS dependent (Fig 1E). By contrast, the degradation of Wpep–GFP did not strictly require ClpS (Fig 1E, open squares), suggesting that Wpep–GFP contains

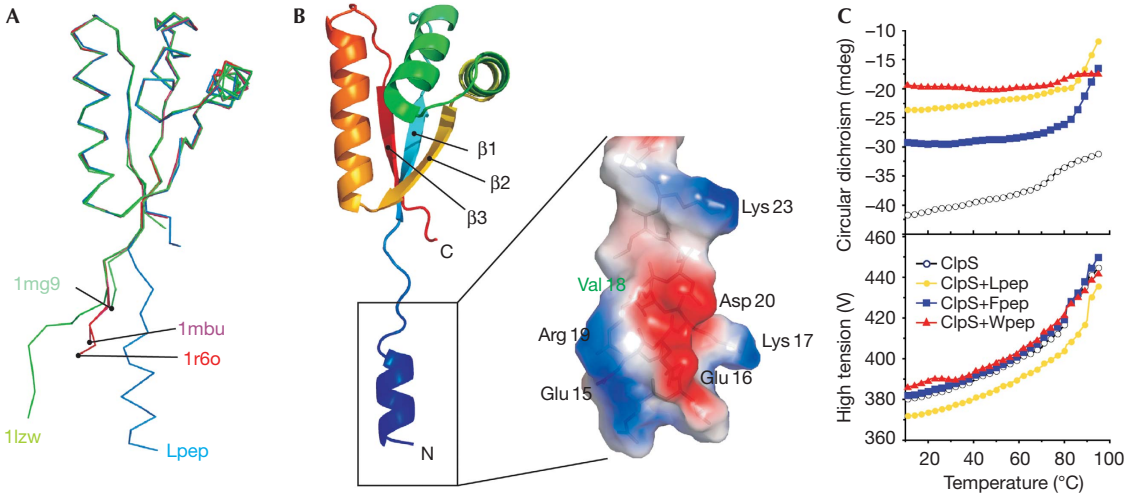

Fig 2 | N-degron binding and ClpS structure. (**A**) The backbone of the ClpS–Lpep complex (Lpep) was superimposed onto four structures of ClpS in complex with the ClpA N-domain, two with wild-type ClpS (1mbu and 1r6o; Guo *et al*, 2002) and two with ClpS(H66A) mutant (1mg9 and 1lzw; Zeth *et al*, 2002). (**B**) Structure of ClpS in complex with Lpep at 1.7 Å resolution (peptide omitted for clarity). The N-terminal helix of ClpS (Glu 15–Lys 23) is boxed and the electrostatic surface shows the distribution of negatively charged (red) and positively charged (blue) regions. (**C**) Thermal melting curves of ClpS (0.02 mM) in the absence of peptide (open circles) or in the presence of Lpep (yellow circles), Fpep (blue squares) or Wpep (red triangles) were drawn at 222 nm.

an intrinsic affinity for ClpA. Moreover, the ClpS-dependent enhancement of Wpep–GFP degradation by ClpAP was also reduced in comparison with the other model substrates—consistent with a weaker affinity of Wpep for ClpS (supplementary Table S1 online). To ensure that the ClpS-mediated delivery of these model substrates was independent of the linker sequence, we also analysed the binding of two other peptides (supplementary Table S1 online; supplementary Fig S1 online) and compared the degradation of Fpep–GFP with two related N-degron–GFP fusion proteins, Lpep2–GFP and Wpep2–GFP, which varied only in their N-terminal residue (supplementary Fig S2 online). Consistent with the above findings, these data indicate that N-end rule substrates bearing an N-terminal Trp bound to ClpS with the lowest affinity and that Wpep, but not Wpep2, contains an internal ClpA-recognition motif. Collectively, these data suggest that ClpS was optimized for the delivery of N-end rule substrates bearing an N-terminal Leu or Phe.

Structural analysis of ClpS

Next, we crystallized ClpS in complex with each N-end rule peptide (supplementary Table S2 online for statistics) and determined the structure of each complex (between 1.7 and 2.9 Å resolution) by using X-ray crystallography. ClpS is a 12-kDa protein with a mixed α/β-fold in which the N-terminal helix (α1) and a compact globular C-terminal domain are separated by a highly flexible random coil structure. To examine any possible structural rearrangements between the free and peptide-bound forms of ClpS, we superimposed four structures of ClpS (Protein Data Bank ID codes: 1mg9, 1lzw, 1mbu, 1r6o) onto the ClpS–Lpep structure (Lpep, Fig 2A). From this analysis, we observed little to no variation (<0.9 Å r.m.s.d.) in the substrate-binding pocket of ClpS on peptide binding. Nevertheless, a substantial change to the N-terminal region of ClpS was observed in the two peptide-bound forms Lpep and Fpep (Fig 2B) of ClpS. In these structures, the N-terminal helix (residues 15–23) was ordered, in contrast to previous structures. Consistently, it has recently been proposed that the N-terminal region of ClpS forms a second site of interaction with ClpA (Hou *et al*, 2008) and, therefore, it is tempting to speculate that substrate binding leads to a conformational change in this highly charged helix, which modulates its interaction with ClpA. To examine the effect of peptide binding, we monitored the thermal stability of ClpS using circular dichroism (CD), in the absence and presence of each peptide (Fig 2C). Surprisingly, ClpS alone showed unusual stability with only a small transition at 70 °C, which could represent unfolding of the N-terminal helix. Interestingly, this transition did not change in the presence of Wpep, although the addition of Fpep or Lpep did alter the melting temperature of ClpS, by approximately 10 °C, consistent with the idea that substrate binding to ClpS could affect the N-terminal helix of ClpS and hence the interaction with ClpA.

Structural analysis of ClpS in complex with an N-degron

In two of the structures—namely ClpS in complex with Lpep (Fig 3A–C) and Fpep (Fig 3D)—all of the residues of the peptide and in the protein–peptide interface were traced unambiguously in at least one molecule of the asymmetric unit because of the formation of contacts with adjacent molecules of the crystal lattice. By contrast, the complex with Wpep was less well defined and only the main chain and side chains of three peptide residues could be traced (Fig 3E). Moreover, the aromatic moiety of the Trp side chain was apparently disordered, as it could not be localized in the electron density. Nevertheless, the binding pocket seems to adapt to the larger side chain and might undergo a limited induced fit mechanism. On the basis of these three crystal structures, a general mode of N-degron binding was deduced for the backbone atoms (Figs 3F and 4D). Four hydrophilic residues, Asn 34, Asp 36, Thr 38 and His 66, clamp the backbone atoms of the first two substrate residues in a stereo-specific manner. The N-terminal

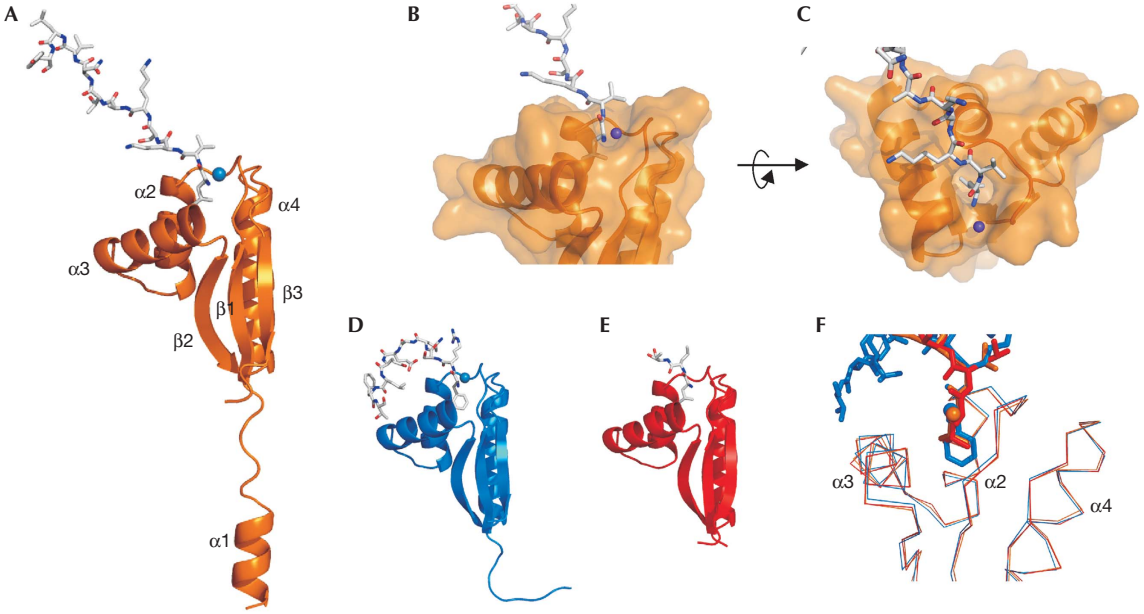

Fig 3 | Structures of ClpS in complex with various N-degron peptides. (**A–C**) The peptide (Lpep, grey) extends away from ClpS (orange). A water molecule (blue sphere) has an important function in complex formation. ClpS is represented as a ribbon (**A**) in complex with Lpep. Surface representation of ClpS binding to Lpep in a side (**B**) and top (**C**) view showing that the amino-terminal side chain is embedded into the surface of ClpS by approximately 8 Å. (**D**) Ribbon diagram showing the complex of ClpS (blue) with Fpep (grey). (**E**) Ribbon diagram showing the structure of ClpS (red) in complex with Wpep (grey). (**F**) A close-up of the backbone of all three complex structures superimposed shows the close alignment of the peptide residues.

nitrogen of the peptide is positioned by Asp 36 (through a conserved water molecule) and Asn 34, whereas the amide nitrogen of the second residue forms a hydrogen bond with Thr 38 (Fig 4D). Interestingly, His 66 forms a hydrogen bond, but not with the α-amino group of the first residue as might be expected; instead, it forms a contact with the carbonyl oxygen of the first residue. This unexpected finding might reflect an important mechanistic detail of substrate binding or might result from the basic pH of the crystallization conditions, which leads to deprotonation of the α-amino group of the substrate. Interestingly, in all of the structures, Asp 35 seems to have another function, as it forms a hydrogen bond with the backbone of Thr 38, stabilizing this residue in specific backbone geometry within the otherwise flexible loop. Consistently, the ClpS double mutant—D35A/D36A—was unable to deliver a model N-end rule substrate to ClpAP for degradation (Erbse *et al*, 2006). Further analysis of the hydrophobic cavity revealed that the nature of the cavity–peptide interaction varies, depending on the side chain of the N-terminal residue of the peptide. For example, Lpep interacts with Met 40 and Met 62 (Fig 4A,B), whereas Fpep interacts with Val 65 (Fig 4C). As expected, all of these residues are highly conserved in most ClpS homologues, including that from *Caulobacter crescentus* (supplementary Fig S3 online).

Met 40 and Met 62 modulate ClpS-binding specificity

Despite the conserved nature of the ClpS-binding pocket, some plasticity is apparent as selected bacterial species have replaced Thr 38 with Asn (Fig 5A). Interestingly, in these species, at least one additional change has also been introduced into the predicted substrate-binding pocket of the protein—for example, the replacement of Asp 36 with Pro—possibly resulting from co-evolution of the binding pocket. These changes to the ClpS protein sequence are largely limited to the *Cyanobacteria* and *Mycobacteria*, and hence might reflect changes to the binding specificity of ClpS in different bacterial species. Intriguingly, only Asp 35 is absolutely conserved between bacterial ClpS and eukaryotic N-recognin protein sequences, whereas N-recognin residues equivalent to Thr 38 and His 66 from *E. coli* ClpS are changed. These modifications to the binding pocket might be instrumental in expanding the substrate specificity of eukaryotic N-recognins or, alternatively, the orientation of the substrate.

To analyse the molecular basis of N-degron recognition, we used our structural model to design several point mutations in the binding pocket of ClpS—that is, H66A, M40A, M62A and a double-mutant M40A/M62A (herein referred to as MAMA)—which is expected to open the binding pocket (compare Fig 5B and C). To monitor the effect of these mutations, we tested the ability of all ClpS mutant proteins to deliver each of the different model N-end rule substrates relative to wild-type ClpS. As expected, H66A was unable to deliver any of the model substrates (Fig 5D, red bars). By contrast, mutations to increase the volume of the binding pocket—M40A, M62A and MAMA—had only a small effect on the rate of Lpep–GFP degradation, which was reduced by up to 40% (Fig 5D), whereas the rate of Fpep–GFP degradation was markedly impaired (Fig 5D) by up to 75% with MAMA. These data suggest that the volume of the ClpS-binding site was optimized for the binding of Phe (and potentially Tyr) and, to a lesser extent, Leu. Consistently, the ClpAP-mediated degradation

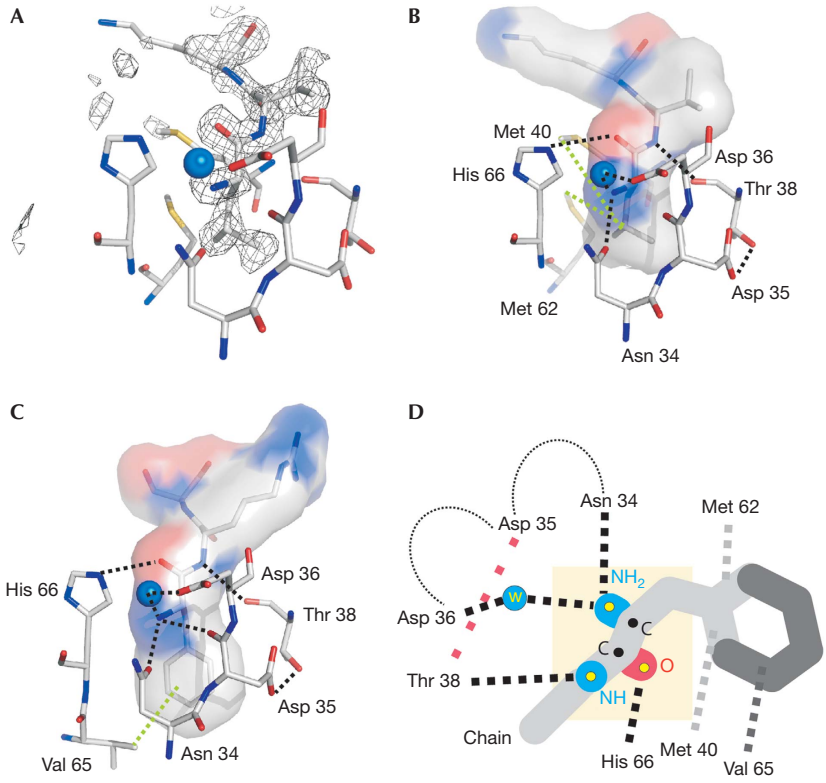

Fig 4 | The N-degron binding site of ClpS. (**A**) Peptide localization (Lpep) based on the $|F_O-F_C|$ difference electron density calculated at 3 σ and a resolution of 1.7 Å. (**B**) Interaction matrix of Lpep seen from the same orientation as (**A**). Residues involved in salt bridges and polar interactions are marked using a black dotted line (<3 Å), whereas hydrophobic interactions (<3.5 Å) with the Leu side chain are indicated by green dotted lines. (**C**) The interaction matrix for Fpep is shown in the same orientation as (**B**) and the interactions are defined as described in (**B**). (**D**) Model showing the overall molecular interactions within the ClpS-binding pocket. Salt bridges and polar interactions common to both structures are indicated by black dotted lines, whereas hydrophobic interactions specific to Leu or Phe are represented by a light or dark grey dotted line, respectively. The stabilizing interaction between Asp 35 and Thr 38 is represented by a pink dotted line.

of Wpep–GFP by M40A and M62A was enhanced (Fig 5D, blue and yellow bars, respectively), suggesting that the enlarged binding pocket of M40A or M62A was able to accommodate the bulky side chain of Trp better than the wild-type ClpS. Conversely, the lateral opening to the side of the binding pocket in MAMA (see Fig 5C) disrupts the binding pocket, negating any potential benefit from a larger binding pocket as can be seen by the rate of Wpep–GFP degradation (Fig 5D). Interestingly, the surface of the putative binding pocket in eukaryotic N-recognins is different in composition from that of bacterial ClpS; for example, in yeast UBR1, Thr is located in the equivalent position as Met 62 in ClpS (see Fig 5A; supplementary Fig S4 online), and hence we speculate that this might provide further lateral space to accommodate the branched side chain of Ile.

Concluding remarks

Although substrate recognition by ClpS is largely restricted to the N-terminal residue alone, the substrate is invariably bound in a stereo-specific manner, making it tempting to speculate that the N-degron is restrained by ClpS in the correct orientation for delivery to the pore of ClpA. Despite the ability of ClpS to bind to and deliver all substrates containing primary destabilizing residues at the N terminus, we propose that the ClpS-binding pocket has been optimized for the recognition of only a subset of these destabilizing residues, notably Phe, Leu and potentially Tyr. Interestingly, Phe and Leu are attached to the N terminus of proteins by LFTR, bearing a secondary destabilizing residue at the N terminus, and hence the physiological role of ClpS might be intimately linked to the activity of LFTR. Identification of natural bacterial N-end rule substrates will help to understand the physiological role of this highly conserved protein.

METHODS

Proteins, peptides and substrate degradation assays. ClpA, ClpP and ClpS (wild type and mutants) were overexpressed in *E. coli* and purified as described previously (Dougan *et al*, 2002; Erbse *et al*, 2008). Recombinant model proteins (Lpep–GFP, Fpep–GFP and Wpep–GFP) were generated using the ubiquitin fusion system (Catanzariti *et al*, 2004). Briefly, proteins were expressed as linear His 6–Ub fusion proteins in *E. coli* strain BL21-CodonPlus(DE3)-RIL (Stratagene, La Jolla, CA, USA) and purified using nickel-nitrilotriacetic acid (Ni-NTA) agarose (Qiagen, Hilden, Germany). The His 6–Ub was cleaved with His 6–Usp2cc (Catanzariti *et al*, 2004), and the untagged proteins were isolated through a reverse affinity chromatography step. All proteins were more than 95% pure as judged by Coomassie-stained

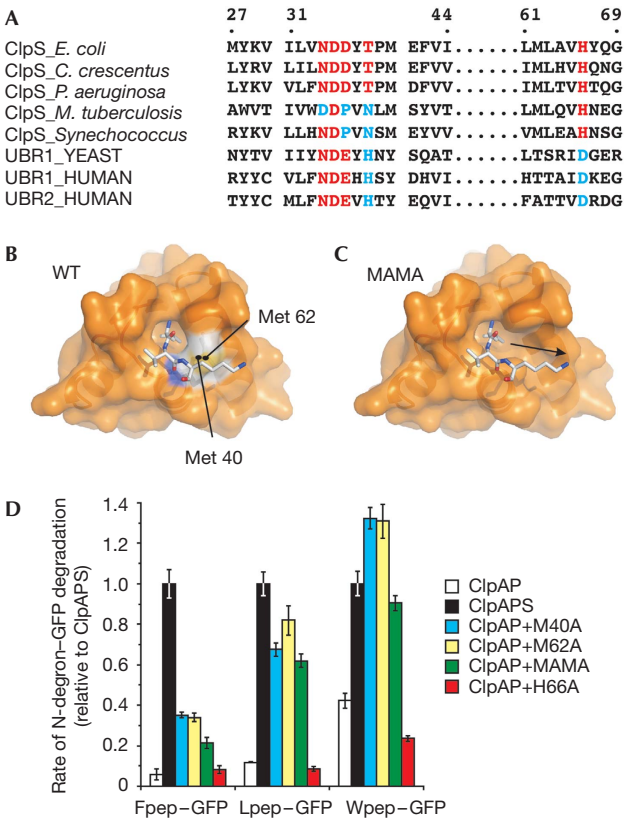

Fig 5 | Met 40 and Met 62 modulate ClpS substrate specificity. (**A**) Sequence alignment of selected ClpS proteins together with the type 2 binding region from eukaryotic UBR1 and UBR2. (**B**,**C**) Surface representation of ClpS (orange) binding to Lpep (grey) showing the top view of (**B**) wild-type (WT) ClpS or (**C**) a model of M40A/M62A (MAMA). (**D**) The rate of ClpAP-mediated degradation of each N-degron–GFP (green fluorescent protein) fusion was monitored by fluorescence in the absence (white bar) or presence of wild-type ClpS (black bars), M40A (blue bars), M62A (yellow bars), MAMA (green bars) or H66A (red bars). Degradation rates were determined relative to the rate of degradation in the presence of wild-type ClpS. Error bars represent the standard error of the mean, from at least five separate experiments.

sodium dodecyl sulphate–polyacrylamide gel electrophoresis. Peptides Fpep (FRSKGEELFT), Lpep (LVKSKATNLLY) and Wpep (WLTMITDSLA) were synthesized by EMC microcollections (Tübingen, Germany) to more than 98% purity. Degradation of all GFP-fusion proteins was monitored by changes in fluorescence (excitation 410 nm and emission 500 nm) on a Spectra Max M2 (Molecular Devices, Sunnyvale, CA, USA). The reactions were carried out using 1.2 μM ClpA, 2.8 μM ClpP and 1.2 μM ClpS (wild type or mutant) as described previously (Dougan *et al*, 2002). The protein concentrations refer to the protomer and were determined using Protein Assay (Bio-Rad, Munich, Germany), with bovine serum albumin (Pierce, Rockford, IL, USA) as a standard.

Biophysical measurements. The peptide solutions were prepared by dissolving the lyophilized peptides in gel filtration (GF) buffer (20 mM HEPES, pH 7.5, 150 mM KCl, 10% (v/v) glycerol). For ITC, the peptide titrations were performed at 30 °C using a VP-ITC microcalorimeter (MicroCal LLC, Northampton, MA, USA). All solutions were degassed using the ThermoVac (MicroCal LLC) accessory instrument of the microcalorimeter, and the reference cell was filled with deionized water. Small volumes (3–4 μl) of peptide solution (0.6, 1 or 2 mM) were injected into a ClpS solution (0.04 or 0.08 mM) in each titration. The first sample injection was removed from the data analysis to avoid possible artefacts that might arise from the diffusion of ligand solution through the injection port during the equilibration of the baseline. To allow each experiment to reach equilibrium, ligand was injected at 300-s intervals. As controls, experiments with buffer, single amino acids (2 mM) or non-N-degron peptides (2 mM) were injected into the ClpS solution. For circular dichroism (CD) spectroscopy, the protein solutions were diluted in GF buffer to 0.02 mM. Thermal melting curves (at 222 nm, between 10 °C and 95 °C) and CD spectra (between 210 and 240 nm) were measured on a Jasco J-810 spectropolarimeter, using 1-mm cuvettes at 0.2 nm resolution, 1 nm bandwith, 1 s time constant and a sensitivity of 100 mdeg.

Crystallization and structure determination. Co-crystals of ClpS in complex with peptides were grown by vapour diffusion (sitting drops) in various conditions (supplementary Table S2 online and supplementary information online for further details). Crystals were transferred to the mother liquor supplemented with 10% polyethylene glycol 400, and flash frozen in liquid nitrogen. Data were collected at the Swiss Light Source (Villigen, Switzerland), beamline PXII at 100 K. Diffraction data were processed using X-ray detection software/XSCALE (Kabsch, 1993). All structures were solved by molecular replacement using the ClpS structure (1MG9). The final models were obtained after several rounds of manual rebuilding and refinement using Coot (Emsley & Cowtan, 2004), REFMAC (Murshudov *et al*, 1997) and PHENIX (http://scripts.iucr.org/cgi-bin/paper?ba5027). The structural geometry of all ligand structures was verified using Procheck (http://www.biochem.ucl.ac.uk/~roman/procheck/procheck.html) and values are given in supplementary Table S2 online. Images were generated using Pymol (http://pymol.sourceforge.net/).

Supplementary information is available at *EMBO reports* online (http://www.emboreports.org)

ACKNOWLEDGEMENTS

We gratefully acknowledge the Max Planck Society, Andrei Lupas and staff of the Max Planck Beamline. We thank Rohan Baker for providing plasmids pHUE and pUsp2cc. D.A.D. and K.N.T. were supported by QEII Fellowships from the Australian Research Council (ARC). V.J.S. is supported by a Max Planck Stipend. S.M.K. is the recipient of a La Trobe University Postgraduate Research Scholarship. This work was supported by a Human Frontier Science Program grant (RGP61/2007) to K.Z. and an ARC Discovery Project (DP0450051) to D.A.D. and K.N.T.

CONFLICT OF INTEREST

The authors declare no conflict of interest.

REFERENCES

Baker TA, Sauer RT (2006) ATP-dependent proteases of bacteria: recognition logic and operating principles. *Trends Biochem Sci* **31:** 647–653

Catanzariti AM, Soboleva TA, Jans DA, Board PG, Baker RT (2004) An efficient system for high-level expression and easy purification of authentic recombinant proteins. *Protein Sci* **13:** 1331–1339

Dougan DA, Reid BG, Horwich AL, Bukau B (2002) ClpS, a substrate modulator of the ClpAP machine. *Mol Cell* **9:** 673–683

Emsley P, Cowtan K (2004) Coot: model-building tools for molecular graphics. *Acta Crystallogr D Biol Crystallogr* **60:** 2126–2132

Erbse A, Schmidt R, Bornemann T, Schneider-Mergener J, Mogk A, Zahn R, Dougan DA, Bukau B (2006) ClpS is an essential component of the N-end rule pathway in *Escherichia coli*. *Nature* **439:** 753–756

Erbse AH, Wagner JN, Truscott KN, Spall SK, Kirstein J, Zeth K, Turgay K, Mogk A, Bukau B, Dougan DA (2008) Conserved residues in the N-domain of the AAA+ chaperone ClpA regulate substrate recognition and unfolding. *FEBS J* **275:** 1400–1410

Guo F, Esser L, Singh SK, Maurizi MR, Xia D (2002) Crystal structure of the heterodimeric complex of the adaptor, ClpS, with the N-domain of the AAA+ chaperone, ClpA. *J Biol Chem* **277:** 46753–46762

Hou JY, Sauer RT, Baker TA (2008) Distinct structural elements of the adaptor ClpS are required for regulating degradation by ClpAP. *Nat Struct Mol Biol* **15:** 288–294

Kabsch W (1993) Automatic processing of rotation diffraction data from crystals of initially unknown symmetry and cell constants. *J Appl Crystallogr* **26:** 795–800

Lupas AN, Koretke KK (2003) Bioinformatic analysis of ClpS, a protein module involved in prokaryotic and eukaryotic protein degradation. *J Struct Biol* **141:** 77–83

Mogk A, Schmidt R, Bukau B (2007) The N-end rule pathway for regulated proteolysis: prokaryotic and eukaryotic strategies. *Trends Cell Biol* **17:** 165–172

Murshudov GN, Vagin AA, Dodson EJ (1997) Refinement of macromolecular structures by the maximum-likelihood method. *Acta Crystallogr D Biol Crystallogr* **53:** 240–255

Soffer RL (1974) Aminoacyl-tRNA transferases. *Adv Enzymol Relat Areas Mol Biol* **40:** 91–139

Tasaki T, Kwon YT (2007) The mammalian N-end rule pathway: new insights into its components and physiological roles. *Trends Biochem Sci* **32:** 520–528

Tobias JW, Shrader TE, Rocap G, Varshavsky A (1991) The N-end rule in bacteria. *Science* **254:** 1374–1377

Varshavsky A (1996) The N-end rule: functions, mysteries, uses. *Proc Natl Acad Sci USA* **93:** 12142–12149

Watanabe K, Toh Y, Suto K, Shimizu Y, Oka N, Wada T, Tomita K (2007) Protein-based peptide-bond formation by aminoacyl-tRNA protein transferase. *Nature* **449:** 867–871

Zeth K, Ravelli RB, Paal K, Cusack S, Bukau B, Dougan DA (2002) Structural analysis of the adaptor protein ClpS in complex with the N-terminal domain of ClpA. *Nat Struct Biol* **9:** 906–911